A Dual Half-Bridge *LLC* Resonant Converter With Magnetic Control for Battery Charger Application

Yuqi Wei, *Student Member, IEEE*, Quanming Luo, *Member, IEEE*, Xiong Du, *Member, IEEE*,
Necmi Altin, *Senior Member, IEEE*, Adel Nasiri, *Senior Member, IEEE*,
and J. Marcos Alonso, *Senior Member, IEEE*

***Abstract*—In this paper, a dual half-bridge *LLC* resonant converter with magnetic control is proposed for the battery charger application. The primary switches are shared by two *LLC* resonant networks, and their outputs are connected in series. One of the *LLC* resonant converters is designed to operate at the series resonant frequency, which is also the highest efficiency operating point, and the constant output voltage characteristic is achieved at this operating point. The second *LLC* resonant converter adopts magnetic control to regulate the total output current and voltage during both constant current charge mode and constant voltage charge mode. Meanwhile, the function decoupling idea is adopted to further improve the system efficiency. The significant amount of the power is handled by the *LLC* resonant converter operating at the series resonant frequency, whereas the second *LLC* resonant converter fulfills the responsibility to achieve closed-loop control. By carefully designing the resonant networks, the zero-voltage switching for primary switches and zero-current switching for secondary diodes can be achieved for whole operation range. A 320-W experimental prototype is built to verify the theoretical analysis, and the maximum efficiency is measured about 95.5%.**

***Index Terms*—Battery charger, LLC resonant converter, magnetic control, soft switching.**

I. INTRODUCTION

NOWADAYS, environmental problems and traditional energy depletion are becoming increasingly serious. Electric vehicles (EVs) have drawn much attention owning to their environmental-friendly characteristic [1]–[3]. The on-board battery charger (OBC) is a crucial technology for the development of EVs. Generally, OBC is a two-stage system, which is composed of a power factor correction circuit and a dc/dc converter. For the dc–dc converter, *LLC* resonant converters have been widely used in this field owning to their features such as: wide input and output voltage range; soft switching capability; and high power density [4]–[18].

For a lithium battery cell, constant current (CC) and constant voltage (CV) charging are required. In order to regulate the output of an *LLC* resonant converter, frequency modulation (FM) or combining FM with phase-shift modulation (PSM) are frequently adopted. In [4]–[11], the FM is applied to regulate the output of the *LLC* resonant converter. The design optimization [9] and the control strategies [7] of the *LLC* resonant converter in the wide output voltage range application is discussed. Specifically, optimized design methodologies for *LLC* resonant converter based on time-weighted average efficiency and based on time-domain analysis are proposed in [11]. However, the main disadvantage of the FM in wide output voltage range applications is that a wide switching frequency range is required. This will cause some problems, such as poor electromagnetic interference (EMI) performance, complicated design of magnetic components, low power density, and high conduction losses. In addition, in order to satisfy the wide output voltage requirement and obtain a low voltage gain, the switching frequency above the series resonant frequency has to be applied. However, in this case, the zero-current switching (ZCS) for the secondary diodes is lost, and this will lead to undesired decrease in efficiency.

In order to narrow the operating frequency range, a control strategy combining the FM and the PSM is proposed in [12]–[15]. Different combination strategies are analyzed and proposed to improve the system efficiency. However, the PSM is not preferred for heavy load conditions due to its high turn-OFF current for the primary switches when compared with the FM. In addition, it still suffers from variable frequency range, and complicates control algorithms. Therefore, the problems of EMI and magnetic components design still remain.

To further narrow the switching frequency range, some topologies based on the modification of an *LLC* converter structure are proposed [16], [17]. However, these topologies require additional switches that operate at hard switching and cause additional power losses. In [18], a dual full-bridge *LLC* resonant converter topology is proposed. An additional switch and a resonant capacitor are required to adjust the operation modes of the *LLC* resonant converter, namely constant output current mode and constant output voltage mode. However, although the constant output voltage mode is verified and has been widely used, the constant output current mode, especially its accuracy, still

---

Manuscript received March 21, 2019; revised May 13, 2019; accepted June 8, 2019. Date of publication June 13, 2019; date of current version November 12, 2019. This work was supported by the National Natural Science Foundation of China under Grant 51577019. Recommended for publication by Associate Editor A. Safaee. *(Corresponding author: Quanming Luo.)*

Y. Wei, Q. Luo, and X. Du are with the State Key Laboratory of Power Transmission Equipment and System Security and New Technology, Chongqing University, Chongqing 400044, China (e-mail: 18332550057@163.com; lqm394@126.com; duxiong@cqu.edu.cn).

N. Altin is with the Department of Electrical and Electronic Engineering, Faculty of Technology, Gazi University, Ankara 06560, Turkey (e-mail: naltin@gazi.edu.tr).

A. Nasiri is with the University of Wisconsin–Milwaukee, Milwaukee, WI 53201 USA (e-mail: nasiri@uwm.edu).

J. M. Alonso is with the Department of Electrical and Electronics Engineering, Universidad de Oviedo, Gijon 33204, Spain (e-mail: marcos@uniovi.es).

Color versions of one or more of the figures in this paper are available online at http://ieeexplore.ieee.org.

Digital Object Identifier 10.1109/TPEL.2019.2922991

See http://www.ieee.org/publications_standards/publications/rights/index.html for more information.

needs to be proved, which will be discussed in Section II. In addition, all of these topologies still need to adopt FM, PSM, or pulsewidth modulation (PWM) to implement closed-loop control. Although the switching frequency range has been reduced, the abovementioned problems are still present.

In addition to FM and PSM, the magnetic control (MC) is also a feasible control strategy for resonant converters. It has been adopted in many applications, including LED drivers, resonant converters, and inverters [19]–[24]. In order to solve the abovementioned problems, in this paper, a dual half-bridge *LLC* resonant converter with MC (or variable inductor control) is proposed. Instead of using FM or PSM, the variable inductor is adopted to regulate the output. Therefore, a constant duty cycle and switching frequency for the primary switches can be achieved, which simplifies the EMI and magnetic components design. Moreover, by carefully designing the resonant networks, the zero-voltage switching (ZVS) operation for primary switches and ZCS operation for secondary diodes can be achieved. Compared with the topology given in [18], the proposed topology has the following advantages.

1) Owning to the MC, constant duty cycle and constant switching frequency for primary switches can be achieved.
2) No additional switch and resonant capacitor are required, thus the system structure is simplified.
3) In addition, switching the capacitor and sudden changes in the resonant capacitor value will result in overshoot or other problems that may damage the converter. In the proposed MC method, the resonant inductor value can be adjusted continuously without abrupt change.
4) The control principle for MC is a simple voltage-controlled current source, which can simplify the control circuit design compared with other control strategies.
5) The function decoupling idea is adopted. One of the *LLC* resonant converters is always operating at the series resonant frequency and handling most of the output power, whereas another *LLC* resonant converter adopts MC to regulate the output so that the averaged efficiency can be improved.

This paper is organized as follows: examinations of constant output voltage and constant output current mode are implemented in Section II. In Section III, the MC strategy is briefly introduced and the operation analysis for the proposed topology is presented. Then, the detailed parameter design procedures are presented in Section IV. Finally, a 320-W experimental prototype is built to verify the theoretical analysis.

II. EXAMINATIONS OF CONSTANT OUTPUT VOLTAGE AND CONSTANT OUTPUT CURRENT MODES OF *LLC* RESONANT CONVERTER

In this part, the constant output voltage and constant output current modes of an *LLC* resonant converter are examined. Fig. 1 shows the topology of a half-bridge *LLC* resonant converter and the converter model obtained by using the fundamental harmonic approximation (FHA) method, where V_{ac} is the fundamental harmonic of the resonant network input voltage and V_{p1} is the fundamental harmonic of the transformer primary side voltage.

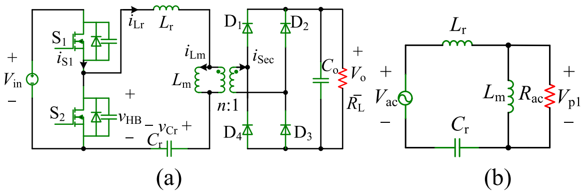

(a) (b)

Fig. 1. Topology of the half-bridge *LLC* resonant converter and its model.

There are two resonant frequencies in an *LLC* resonant converter. First one is the series resonant frequency f_r, which is determined by resonant capacitor C_r and resonant inductor L_r. The second one is the parallel resonant frequency f_m, which is determined by resonant capacitor C_r, resonant inductor L_r, and magnetizing inductor L_m. Both resonant frequencies are given by the following equations:

$$f_r = \frac{1}{2\pi\sqrt{L_r C_r}} \tag{1}$$

$$f_m = \frac{1}{2\pi\sqrt{(L_r + L_m)C_r}}. \tag{2}$$

Theoretically, at the series resonant frequency, the output voltage of the *LLC* resonant converter is independent of load, and at the parallel resonant frequency, the output current is independent of load. In the following part, the theoretical analysis will be discussed, and the experimental results will be used to examine the accuracy of the constant output voltage and constant output current characteristics. In this research, the resonant inductor is separated from the transformer, so the leakage inductance is very small compared with the magnetizing inductance and resonant inductance, which makes the secondary leakage inductance effects ignorable. However, if the integrated transformer is adopted, where the secondary leakage inductance is not small anymore, its effects must be analyzed as presented in [25] and [26]. Therefore, in this research, the secondary leakage inductance effects are ignored.

A. Constant Output Voltage Mode

Based on Fig. 1(b), the output voltage of the *LLC* resonant converter can be derived according to the voltage divider law as follows:

$$V_{p1}(s) = V_{\mathrm{ac}} \frac{\frac{L_m s R_{\mathrm{ac}}}{L_m s + R_{\mathrm{ac}}}}{L_r s + \frac{1}{C_r s} + \frac{L_m s R_{\mathrm{ac}}}{L_m s + R_{ac}}} \tag{3}$$

$$R_{\mathrm{ac}} = \frac{8n^2}{\pi^2} R_L \tag{4}$$

$$V_{p1} = \frac{2\sqrt{2}n}{\pi} V_o \tag{5}$$

$$V_{\mathrm{ac}} = \frac{\sqrt{2}}{\pi} V_{\mathrm{in}}. \tag{6}$$

At the series resonant frequency, resonant capacitor C_r is resonating with the resonant inductor L_r, so the term

TABLE I
CONVERTER PARAMETERS

Unit	Components	Parameters
Half-bridge LLC resonant converter	Resonant capacitor C_r	26.2 *n*F
	Resonant inductor L_r	96 µH
	Magnetizing inductor L_m	230 µH
	Turns ratio *n*	2.5:1
	Series resonant frequency f_r	100 kHz
	Parallel resonant frequency f_m	54 kHz
	Input voltage	100 V

$(1/C_r s + L_r s)$ equals 0. Then, (3) can be simplified as

$$V_o(s) = \frac{V_{\text{in}}}{2n}. \tag{7}$$

Based on (7), it can be seen that at the series resonant frequency, the output voltage is independent of the load, so it is in the constant output voltage mode.

B. Constant Output Current Mode

By dividing both sides of (3) by R_{ac} and rearranging the result, one can obtain

$$I_o(s) = nV_{\text{ac}} \frac{1}{\left(L_r s + \frac{1}{C_r s}\right) + \frac{R_{\text{ac}}}{L_m s}\left(L_m s + L_r s + \frac{1}{C_r s}\right)}. \tag{8}$$

At the parallel resonant frequency, resonant capacitor C_r and resonant inductor L_r are resonating with magnetizing inductor L_m, so the term $(L_m s + L_r s + 1/C_r s)$ equals 0. Then, (8) can be simplified as

$$I_o(s) = \frac{nV_{\text{ac}}}{L_r s + \frac{1}{C_r s}}. \tag{9}$$

It can be seen that the output current is independent of the load for this condition.

C. Examination of Constant Output Voltage and Constant Output Current Modes

In order to examine the constant output voltage and constant output current characteristics, an *LLC* resonant converter with the parameters shown in Table I is built.

According to (7), at the series resonant frequency, the output voltage is kept constant at 20 V, by taking diode forward voltage into consideration, and the output voltage should be kept constant at 19 V. Fig. 2 shows the experimental waveforms including the input voltage V_{in}, the resonant inductor current i_{Lr}, the output voltage V_o, and the output current I_o at series resonant frequency with different loads.

By substituting $s = 2\pi f_s j$ (where $f_s = f_m$) into (9), one can calculate that the theoretical constant output current is 1.29 A. Fig. 3 shows the experimental waveforms when the converter is operating at parallel resonant frequency with different loads.

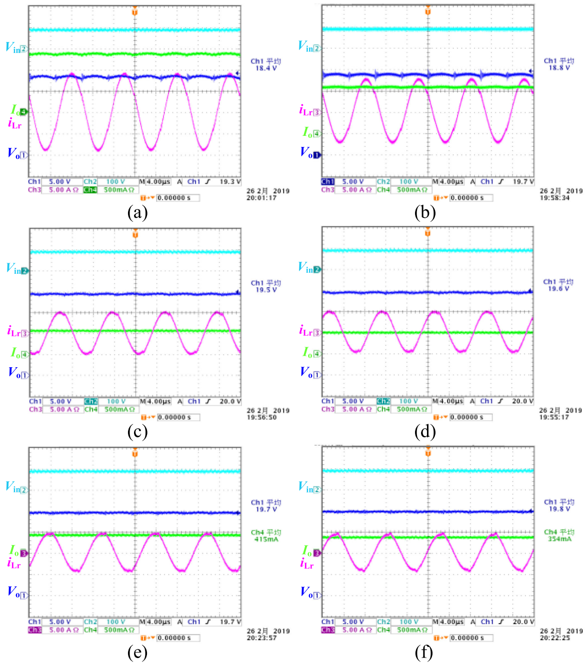

Fig. 2. Experimental waveforms at series resonant frequency operating point with different loads. (a) $R_L = 15\,\Omega$. (b) $R_L = 20\,\Omega$. (c) $R_L = 50\,\Omega$. (d) $R_L = 60\,\Omega$. (e) $R_L = 80\,\Omega$. (f) $R_L = 110\,\Omega$.

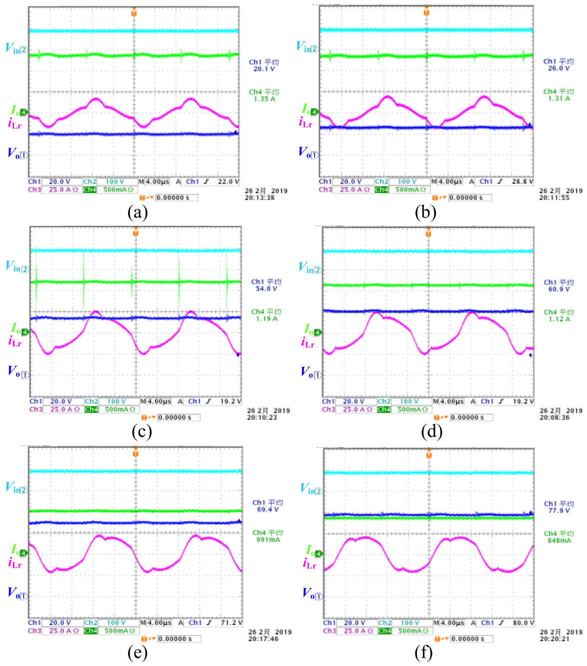

Fig. 3. Experimental waveforms at parallel resonant frequency operating point with different loads. (a) $R_L = 15\,\Omega$. (b) $R_L = 20\,\Omega$. (c) $R_L = 50\,\Omega$. (d) $R_L = 60\,\Omega$. (e) $R_L = 80\,\Omega$. (f) $R_L = 110\,\Omega$.

The accuracies of the constant output voltage and constant output current modes are obtained by calculating the relative error of the theoretical value and experimental value as illustrated in Fig. 4. It can be seen that the accuracy of constant output voltage mode is much higher than that of the constant output current mode, and the accuracy varies slightly with the load.

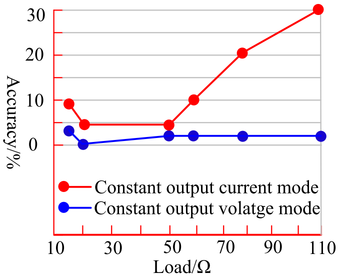

Fig. 4. Accuracy comparison between constant output voltage mode and constant output current mode.

In comparison with the constant output voltage characteristic, the constant output current characteristic has considerable errors, which will finally lead to a relatively wide switching frequency range to keep the output current constant. This phenomenon can easily be understood by examining the principle of the FHA method, only the fundamental harmonic is considered. When the switching frequency is close to the series resonant frequency, the resonant current is more sinusoidal and FHA provides more accurate results. However, when the switching frequency is away from the series resonant frequency, the waveform is distorted and many harmonics are added (see Fig. 3), which leads to the poor accuracy of the constant output current mode. In addition, if the *LLC* resonant converter operates at parallel resonant frequency, the ZVS operation for the primary switches is lost, which is not preferred for MOSFETs. In [18], both the constant output current and constant output voltage modes are adopted. However, due to the poor accuracy of the constant output current characteristic, a relatively wide switching frequency operation range is still required. Because of the high accuracy of the constant output voltage mode at the series resonant frequency operating point, only this mode is used in the proposed topology.

III. OPERATION ANALYSIS AND DESIGN CONSIDERATIONS FOR THE PROPOSED CONVERTER

In this part, the operation principle of the MC is briefly introduced, and then, the operation analysis for the proposed converter is presented. Finally, based on the battery charging profile, the design considerations for the proposed converter are elaborated.

A. Introduction of Magnetic Control

The structure of the variable inductor using a double E-core is shown in Fig. 5. The control winding or auxiliary winding is divided into two identical portions with the number of turns N_{DC}, which is mounted on the lateral legs of the core. The inductor winding or main winding with the number of turns N_{AC} is placed on the air-gapped middle leg of the core. The dc bias current allows for the modification of the inductance of the main winding. The typical relationship between dc bias current and variable inductance value is shown in Fig. 6. It can be seen that the variable inductance value is inversely proportional to the dc bias current.

In the proposed method, the inductance value of the variable inductor is controlled. The control scheme is shown in Fig. 7.

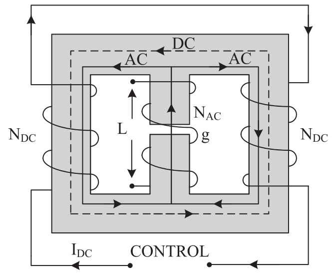

Fig. 5. Structure of the variable inductor.

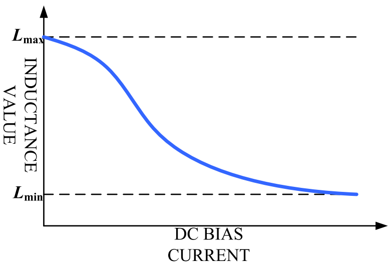

Fig. 6. Inductance value versus dc bias current of a variable inductor.

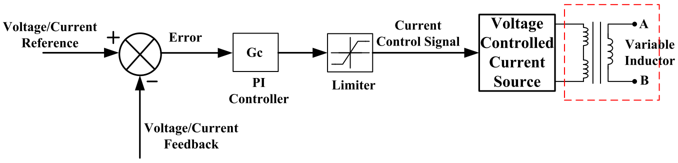

Fig. 7. Control scheme of the system.

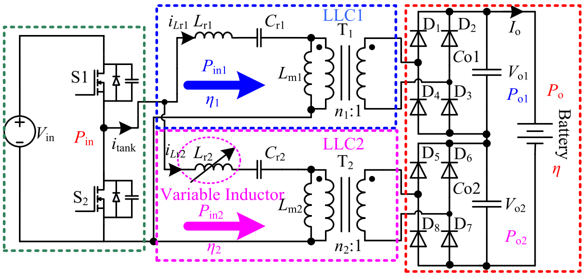

Fig. 8. Topology of the proposed converter.

During the CC charge mode, the error is obtained by comparing the reference current and the feedback current, and then applied to the proportion integration (PI) controller. Similarly, during the CV charge mode, the error is obtained by comparing the reference voltage and the feedback voltage and then the error is applied to the PI controller. The PI controller generates the control signal that is used to adjust the dc bias current. Consequently, the inductance value of the variable inductor is adjusted to regulate the output current or voltage of the second *LLC* resonant converter.

B. Operation Analysis of the Proposed Converter

The proposed converter is shown in Fig. 8. The converter mainly includes the following parts:

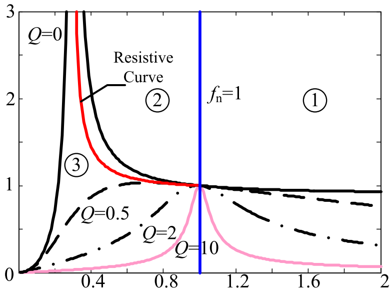

Fig. 9. Voltage gain with normalized switching frequency f_n and quality factor Q.

1) half-bridge inverter, which is shared by two *LLC* resonant converters;
2) two *LLC* resonant networks, LLC_1 operates at the fixed operating point, whereas LLC_2 adopts MC to regulate the output; and
3) two rectifier networks, which are connected in series in order to reduce the voltage stress on each diode.

Therefore, a low-voltage rating diode can be selected to achieve higher efficiency.

Fig. 9 shows the voltage gain curves versus normalized switching frequency $f_n (f_n = f_s/f_r)$ for different quality factor Q $(Q = \sqrt{L_r/C_r}/R_{\text{ac}})$ values, where the resistive curve is the operating points when resonant network input current is in phase with its input voltage. It can be seen that the line $f_n = 1$ and the resistive curve have divided the *LLC* resonant converter operation into three regions, namely region 1, region 2, and region 3. It is well known that in region 1, ZVS operation for primary switches is achieved, but ZCS operation for secondary diodes is lost. For region 2, both ZVS operation for primary switches and ZCS operation for secondary diodes can be achieved. For region 3, ZCS operation for primary switches and secondary diodes are achieved. Since MOSFETs are preferred to operate under ZVS, region 2 is the most suitable operation region for the *LLC* resonant converter. Operation in region 2 can be guaranteed if: the switching frequency is below or equal to the resonant frequency; and the voltage gain is monotonously decreasing with the increase in normalized switching frequency within the operating range.

In addition, a lower f_n leads to a higher voltage gain. Similarly, a lower Q results in a higher voltage gain. For the MC, the switching frequency is fixed, whereas the resonant inductance is adjustable, which means that the series resonant frequency is not constant. So, the normalized switching frequency is adjustable. At the CC charge mode, the output voltage is increasing and a higher voltage gain is required. Therefore, the variable inductance value is reduced to increase the series resonant frequency and reduce the normalized switching frequency, finally increasing the voltage gain and keeping the output current constant. At CV charge mode, the output voltage needs to be kept constant while the quality factor Q is reducing during the CV charge stage and the voltage gain is increased. So, the variable inductance value should be increased to reduce the series resonant frequency and increase the normalized switching frequency, thus finally keeping the voltage gain and the output voltage constant.

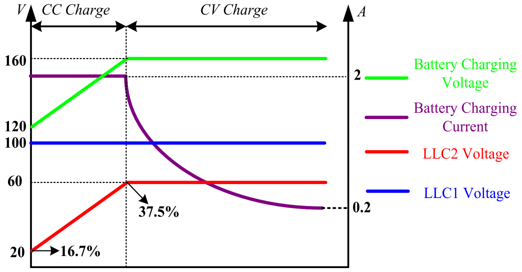

Fig. 10. Battery charging profile.

During the whole operation range, LLC_1 is designed to operate at the series resonant frequency point, where its output voltage is almost kept constant.

C. Design Considerations for the Proposed Converter

Before the discussion of the design considerations, the battery charging profile is introduced. The starting voltage value of a battery cell is 3.2 V, the end voltage value is 4.2 V, and the charging current is 2 A. The battery pack is composed of 38 battery cells connected in series. The battery pack charging profile and the voltage distribution between LLC_1 and LLC_2 are shown in Fig. 10. It can be seen that LLC_1 is designed to operate at the series resonant frequency and its output voltage keeps constant. The function decoupling idea is adopted here to further improve the system efficiency. The principle for determining the power distribution between two *LLC* resonant networks can be described as the following: as shown in Fig. 8, where $P_{\text{in}1}$ and P_{o1} represent the input power and output power of the LLC_1, and $P_{\text{in}2}$ and P_{o2} represent the input power and output power of LLC_2, and the efficiencies of LLC_1 and LLC_2 are represented by η_1 and η_2, respectively. Based on the energy conservation law, the following equations can be obtained:

$$P_{o1} = \eta_1 P_{\text{in}1} \tag{10}$$

$$P_{o2} = \eta_2 P_{\text{in}2}. \tag{11}$$

Then, the total output power of the proposed converter can be expressed as follows:

$$P_o = P_{o1} + P_{o2} = P_{o1} = \eta_1 P_{\text{in}1} + \eta_2 P_{\text{in}2}. \tag{12}$$

The system efficiency can be derived as follows:

$$\begin{aligned}\eta &= \frac{P_o}{P_{\text{in}}} = \frac{\eta_1 P_{\text{in}1} + \eta_2 P_{\text{in}2}}{P_{\text{in}1} + P_{\text{in}2}} \\ &= \eta_1 \frac{P_{\text{in}1}}{P_{\text{in}1} + P_{\text{in}2}} + \eta_2 \frac{P_{\text{in}2}}{P_{\text{in}1} + P_{\text{in}2}} = \eta_1 m_1 + \eta_2 m_2\end{aligned} \tag{13}$$

where m_1 and m_2 are the percentile power distributions of LLC_1 and LLC_2, respectively, and $m_1 + m_2 = 1$.

Based on (13), the system efficiency is related to the parameters m_1, m_2, η_1, and η_2. In this research, LLC_1 is designed to operate at the series resonant frequency operating point, which is also the best efficiency operating point for an *LLC* resonant converter; while the responsibility of LLC_2 is to regulate the output of the whole system, so its operating point varies, which will reduce the corresponding efficiency η_2. This viewpoint is

TABLE II
SYSTEM SPECIFICATIONS

Parameter	Designator	Value
Input voltage	$V_{\mathrm{i,min}}$-$V_{\mathrm{i,max}}$	340 V-380 V
Output voltage	V_{o}	120 V-160 V
Output power	$P_{\mathrm{o,min}}$-$P_{\mathrm{o,max}}$	32 W-320 W
Switching frequency	f_{s}	100 kHz

also verified by the efficiency curve of the proposed converter as shown in the experimental results. Therefore, theoretically, to maximize the overall system efficiency, parameter m_1 should be close to 1, which means LLC_1 should handle most of the output power. However, the output voltage of LLC_2 is required to achieve the closed-loop regulation. In addition, a small output voltage of LLC_2 will lead to a high step-down turns ratio when considering the high input voltage (340–380 V), which will also degrade the converter efficiency. Overall, the main considerations for the power sharing between two *LLC* resonant networks are: overall system efficiency, which requires a small output voltage of LLC_2; and appropriate turns ratio of LLC_2, which avoids a very small output voltage. In this research, a compromise between (1) and (2) is made. The minimum output voltage of LLC_2 is designed to be 20 V, and the percentile power distribution of LLC_1 is 62.5% or 37.5% for LLC_2.

The specifications of the proposed converter are summarized in Table II. Input voltage equals 360 V, which is selected as the nominal operating point.

1) Design Considerations for LLC$_2$: Since LLC_1 is operating at the series resonant frequency, which is much easier to design, the design procedures begin with LLC_2. The design guidelines for LLC_2 are summarized as follows: First, the secondary diodes can achieve ZCS operation, which requires a switching frequency lower than the series resonant frequency during the whole operation range; and second, the voltage gain of LLC_2 can satisfy the system voltage gain requirement, and the voltage gain is monotonously decreasing with the increase in the normalized switching frequency.

First, in order to guarantee the ZCS operation for secondary diodes, the series resonant frequency operation is designed at the beginning of the CC charge when the resonant inductor reaches its maximum value. Based on the input voltage and output voltage at the beginning of the CC charge, the transformer turns ratio can be calculated as follows:

$$n_1 = \frac{V_{\mathrm{in,max}}}{2V_{o1}} = \frac{190}{100} = 1.9 \tag{14}$$

$$n_2 = \frac{V_{\mathrm{in,max}}}{2V_{o2,\mathrm{min}}} = \frac{190}{25} = 7.6. \tag{15}$$

The voltage stress should be considered when designing resonant capacitor C_{r2}. Equation (16) represents the voltage stress on the resonant capacitor. The voltage stress is selected as 400 V, and the resonant capacitor of 24.7 nF is selected.

$$V_{\mathrm{cr,max}} = \frac{V_{\mathrm{in,min}}}{2} + \frac{V_o^2}{2R_{L,\mathrm{min}} f_s V_{\mathrm{in,min}} C_{r,\mathrm{min}}}. \tag{16}$$

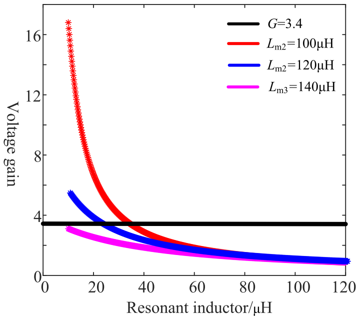

Fig. 11. Voltage gain with a resonant inductor under different magnetizing inductor values.

As mentioned above, when the resonant inductor reaches its maximum value, the series resonant frequency should be equal to the switching frequency, which can guarantee the ZCS operation for the secondary diodes during the whole operation range. Based on (17), $L_{r,\mathrm{max}}$ equal to 102 μH is calculated and

$$f_s = f_{r2} = \frac{1}{2\pi\sqrt{L_{r,\mathrm{max}} C_{r2}}}. \tag{17}$$

Next, we need to find the suitable magnetizing inductor value and minimum resonant inductor value to satisfy the system voltage gain requirement. Based on the battery charging profile, the maximum voltage gain is calculated as follows:

$$G_{\mathrm{max}} = \frac{\left(V_{o,\mathrm{max}} - \frac{V_{\mathrm{in,min}}}{n_1}\right) \times n_2}{V_{\mathrm{in,min}}} = \frac{\left(160 - \frac{170}{1.9}\right) \times 7.6}{170} = 3.38. \tag{18}$$

At the beginning of the CC charge mode, the equivalent load is the smallest one, and this is also the worst condition for the converter to achieve the desired voltage gain. Fig. 11 shows the voltage gain curve of LLC_2 with different resonant inductor and magnetizing inductor values under the worst condition. It can be seen that the voltage gain is monotonously decreasing with the increase in the normalized switching frequency under these conditions, so LLC_2 is operating in region 2. In order to satisfy the system voltage gain requirement, a lower magnetizing inductor is preferred. However, a lower L_m results in a high-resonant rms current and high conduction losses. Therefore, a compromised magnetizing inductor value of 120 μH is selected. Then, the minimum resonant inductor value of 27 μH can be found based on Fig. 12 to meet the maximum voltage gain requirement. Up to now, the resonant network for LLC_2 has been finalized: $C_{r2} = 24.7$ nF, $L_{r2} = 27$–$102\,\mu$H, and $L_{m2} = 120\,\mu$H.

2) Design Considerations for LLC$_1$: Clearly, for LLC_1, it is always operating in region 2. Similarly, based on the voltage stress requirement, a resonant capacitor value of 66 nF is selected. Since LLC_1 is operating at the series resonant frequency point, the resonant inductor L_{r1} can be calculated based on the following equation

$$fs = fr1 = \frac{1}{2\pi\sqrt{Lr1Cr1}}. \tag{19}$$

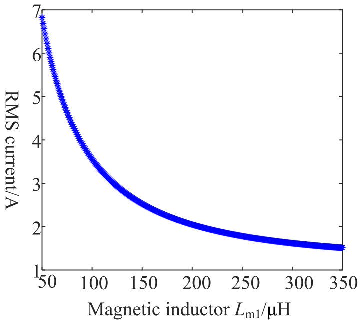

Fig. 12. Relationship between magnetizing inductor L_{m1} and resonant network rms current.

So, $L_{r1} = 38\ \mu$H is selected. For magnetizing inductor L_{m1}, the design considerations mainly include two aspects: First, rms value of the resonant network current should be low; and second, total input impedance of the resonant tank should be inductive.

The relationship between magnetizing inductor L_{m1} and the resonant network rms current is shown in Fig. 12. It can be seen that higher magnetizing inductance value leads to a lower resonant network rms current. In addition, when the magnetizing inductance value is higher than 200 μH, the current decreasing slope becomes low, so L_{m1} equal to 200 μH is selected. Next, the total input impedance will be examined.

Because of the parallel connection of two *LLC* resonant networks, the total input impedance can be expressed as follows:

$$Z_{\text{in}} = Z_{\text{in1}} // Z_{\text{in2}} \tag{20}$$

where Z_{in1} is the input impedance of LLC_1 and Z_{in2} is the input impedance of LLC_2.

Since LLC_1 is operating at the series resonant frequency, the input impedance of LLC_1 can be simplified as

$$Z_{\text{in1}} = \frac{L_{m1} s R_{\text{ac1}}}{L_{m1} s + R_{\text{ac1}}} \tag{21}$$

For *LLC*2, the input impedance can be expressed as below

$$Z_{\text{in2}}(s) = L_{r2} s + \frac{1}{C_{r2} s} + \frac{L_{m2} s R_{\text{ac2}}}{L_{m2} s + R_{\text{ac2}}}. \tag{22}$$

Based on (20)–(22), one can find the relationship among resonant tank input impedances Z_{in1}, Z_{in2}, and Z_{in} and the resonant variable inductor L_{r2} as shown in Fig. 13. Similarly, the worst condition (at the beginning of the CC charge, where the converter is the least inductive) for the converter is checked. It can be seen that during the whole operation range, the total input impedance angle is positive, which means that the converter is operating in inductive region, agreeing with the theoretical analysis. Thus, the primary switches can achieve the ZVS operation. The parameters for LLC_1 are: $C_{r1} = 66$ nF, $L_{r1} = 38\ \mu$H, and $L_{m1} = 200\ \mu$H.

IV. EXPERIMENTAL RESULTS

In this part, an experimental prototype is built to verify the theoretical analysis. The experimental setup is shown in Fig. 14. The system mainly includes the following parts:

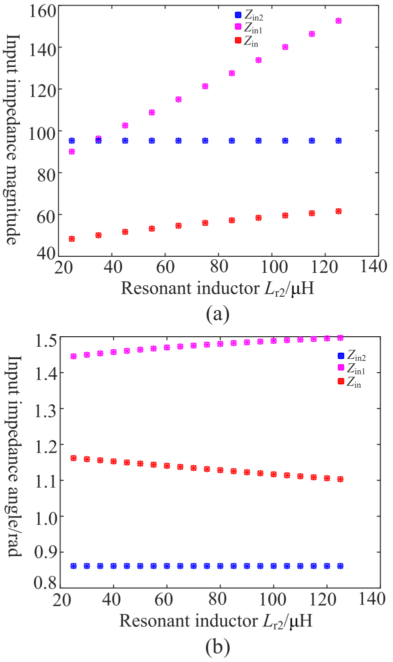

(a)

(b)

Fig. 13. Relationship between input impedance and resonant variable inductor L_{r2}. (a) Magnitude information. (b) Angle information.

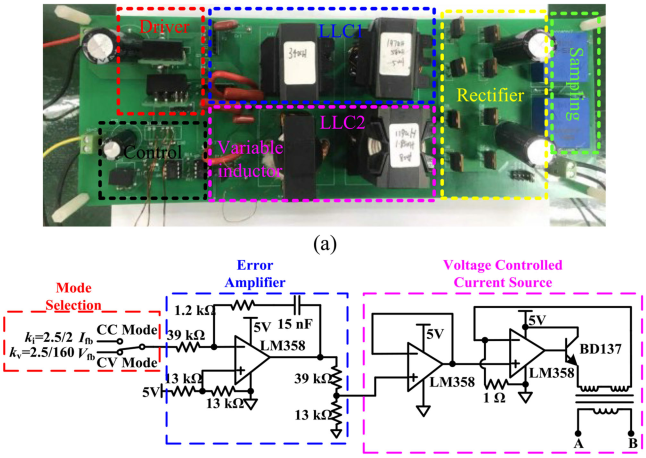

(a)

(b)

Fig. 14. Experimental setup of the dual half-bridge *LLC* resonant converter with MC. (a) Experimental setup. (b) Control circuit.

1) main power circuit;
2) voltage and current sampling circuit, where LV 25-P and LA 25-NP from life energy motion (LEM) are adopted to sample the output voltage and output current, respectively;
3) a control circuit, where LM358 is adopted to form a PI controller, and combined with NPN transistor BD137, a voltage controlled current source is built to provide the dc bias current for the variable inductor; and
4) auxiliary power supply, which is designed to make a control circuit, a voltage sampling circuit, and a driver circuit work.

TABLE III
CIRCUIT PARAMETERS AND COMPONENTS' PART NUMBERS

Unit	Components	Parameters
Dual half-bridge LLC resonant converter with magnetic control	Resonant capacitor C_{r1}	66 *n*F
	Resonant inductor L_{r1}	38 μH
	Magnetizing inductor L_{m1}	200 μH
	Transformer turns ratio n_1	1.9
	Output capacitor C_{o1}	150 μF
	Resonant capacitor C_{r2}	24.7 *n*F
	Resonant variable inductor L_{r2}	26 μH-102 μH EE42 PC40 N_{DC}=45, N_{AC}=10 g=0.7 mm
	Magnetizing inductor L_{m2}	120 μH
	Transformer turns ratio n_2	7.6
	Output capacitor C_{o2}	150 μF
	Switches S_1, S_2	IPP65R065C7
	Rectifier diodes	VFT5202

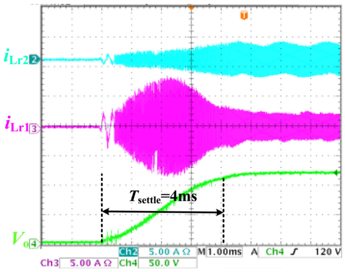

Fig. 15. Soft start-up process of the proposed converter.

In practice, the leakage inductance of the transformer can be utilized as part of the variable inductor, so the design requirements for transformer are reduced. Circuit parameters and components part numbers are given in Table III.

Similarly to the traditional *LLC* resonant converter [27], the soft start-up mechanism can be described as follows. The switching frequency during the start-up process is decreased from a high switching frequency (three times higher than the nominal operating frequency) to the nominal switching frequency to reduce the current spike. Fig. 15 shows the soft start-up process of the proposed topology. It can be seen that the output voltage builds smoothly and quickly. The total settling time is about 4 ms.

Fig. 16 shows the relationship between the designed variable inductor value and dc bias current. The blue line shows the simulation results by using the model in [21] and the red line shows the obtained experimental results. It can be seen that the experimental results agree with the simulation results, and the dc bias current is set as 0–0.5 A to satisfy the required inductance range.

First, the operation of LLC_1 is tested individually. Fig. 17 shows the open-loop experimental waveforms of the output voltage V_{o1}, output current I_{o1}, resonant inductor current i_{Lr}, and resonant tank input voltage $V_{\rm HB}$ of LLC_1 with different output power when input voltage equals 380 V. It can be seen that

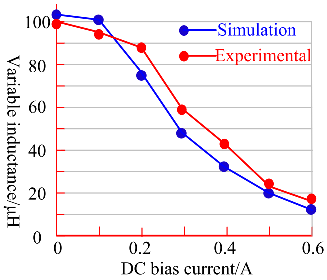

Fig. 16. Relationship between dc bias current and variable inductance value.

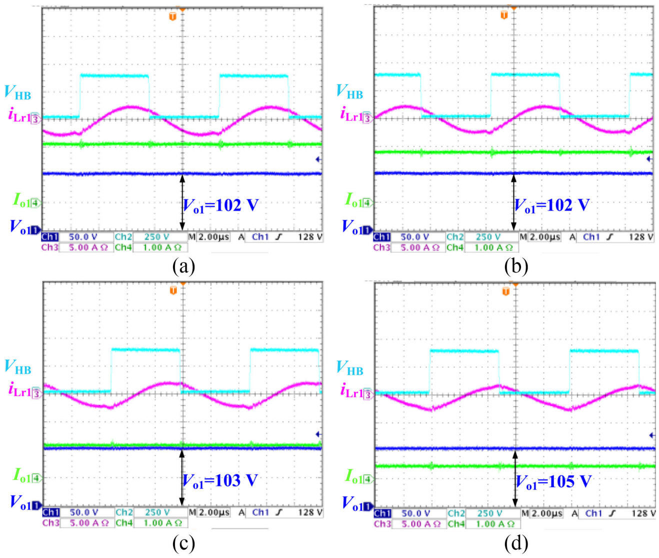

(a) (b)
(c) (d)

Fig. 17. Open-loop experimental waveforms when LLC_1 operating individually at different output powers. (a) $P_o = 200$ W. (b) $P_o = 170$ W. (c) $P_o = 100$ W. (d) $P_o = 25$ W.

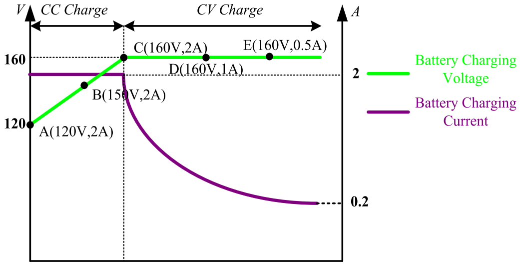

Fig. 18. Five operating points from the battery charging profile.

the output voltage of LLC_1 remains constant at 100 V with different output power, which agrees with the theoretical analysis. Therefore, LLC_1 is designed to operate at the series resonant frequency operating point, where its output voltage almost remains constant with different output power.

Then, the experimental waveforms of the proposed dual half-bridge *LLC* resonant converter with MC are presented. The experimental waveforms are obtained for $V_{\rm in} = 360$ V, which is the nominal operating point in this research. Five operating points from the battery charging profile are selected and depicted in Fig. 18.

The left of Fig. 19(a) shows the experimental waveforms of the resonant tank input voltage $V_{\rm HB}$, input current $i_{\rm tank}$ (which

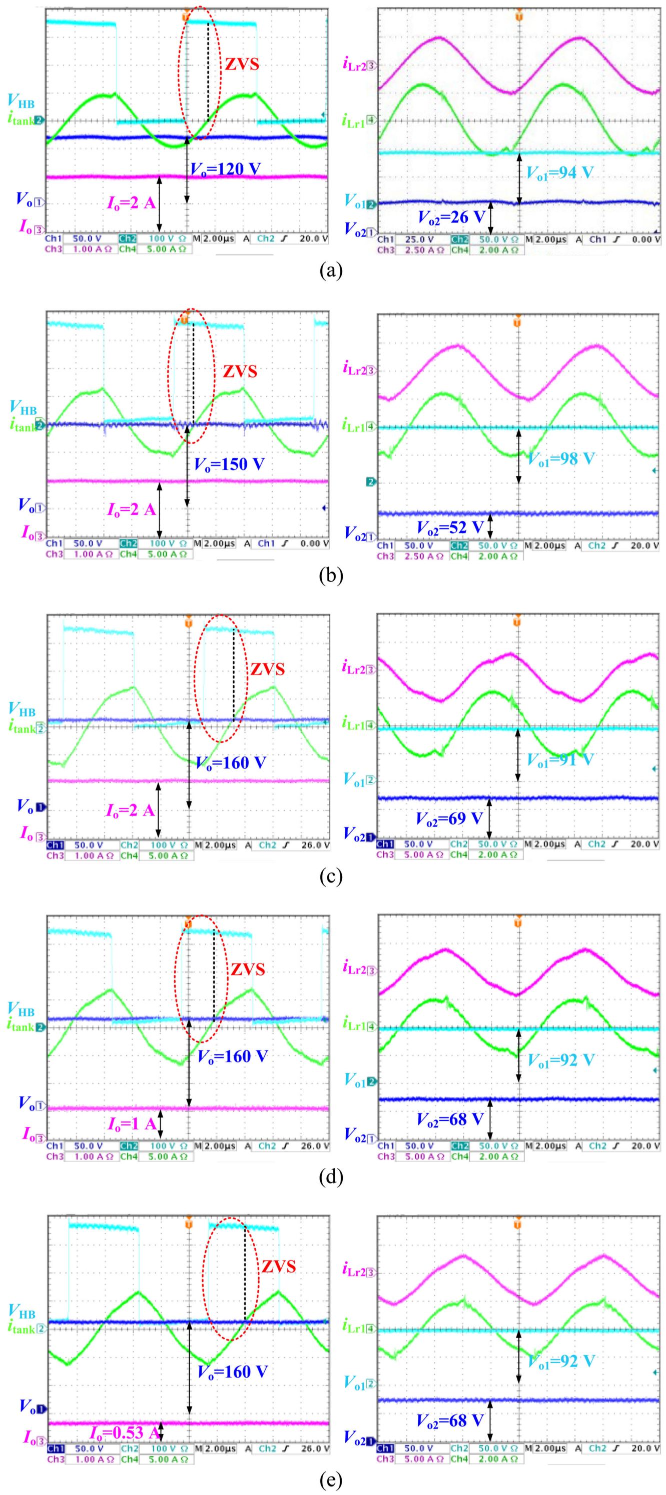

(a)

(b)

(c)

(d)

(e)

Fig. 19. Experimental waveforms. (a) Operating point A. (b) Operating point B. (c) Operating point C. (d) Operating point D. (e) Operating point E.

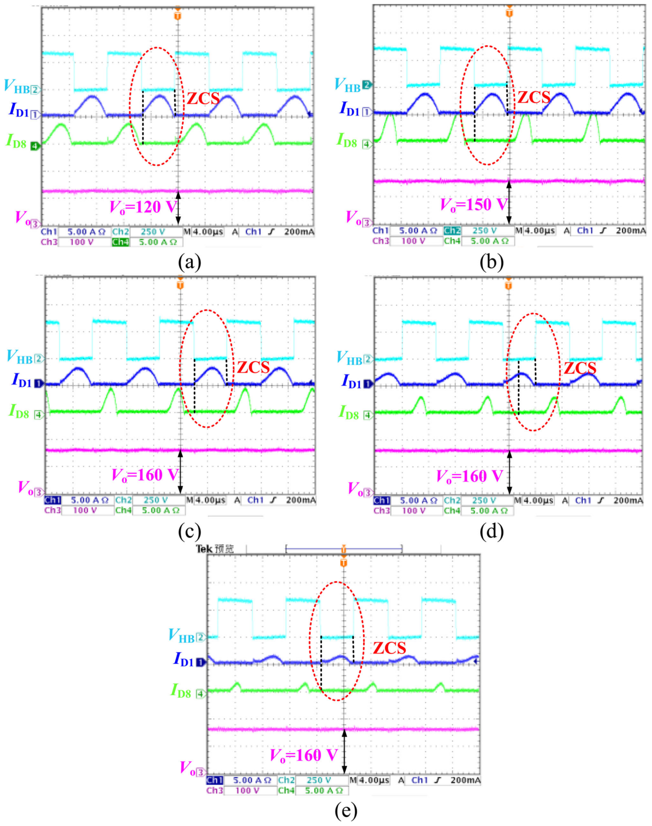

(a)

(b)

(c)

(d)

(e)

Fig. 20. Experimental waveforms of diode currents I_{D1} of LLC_1 and I_{D8} of LLC_2, resonant tank input voltage V_{HB}, and output voltage V_o. (a) Operating point A. (c) Operating point B. (c) Operating point C. (d) Operating point D. (e) Operating point E.

equals i_{Lr1} plus i_{Lr2}), output voltage V_o and output current I_o of operating point A, and the right one shows the output voltage and resonant inductor current of LLC_1 and LLC_2. It can be seen that the output current and output voltage can meet the requirement, and the resonant tank input current lags behind the resonant tank input voltage. So, the converter is operating in inductive region, and the ZVS operation for the primary switches is achieved.

Similarly, Fig. 19(b) shows the experimental waveforms of operating point B. The output current is constant at 2 A, and the resonant tank input current is lagging behind the input voltage. So, the ZVS operation for the primary switches is achieved.

Fig. 19(c) shows the experimental waveforms of operating point C, which is also the transition point from CC charge mode to CV charge mode. At this operating point, the output current is still kept constant at 2 A, whereas the output voltage reaches its maximum value of 160 V. In addition, the ZVS operation is still maintaining in this condition.

Fig. 19(d) shows the experimental waveforms of operating point D, which is located in CV charge mode. At this operating point, the output voltage is constant at 160 V, whereas the output current decreases to 1 A. The primary switches still operate at ZVS.

Fig. 19(e) shows the experimental waveforms of operating point E. Obviously, the output voltage keeps constant at 160 V, and the output current equals 0.53 A. The resonant tank input current is still lagging behind the input voltage, and thus the ZVS operation can be achieved for the primary switches.

Fig. 20 shows the experimental waveforms of the diode currents I_{D1} of LLC_1 and I_{D8} of LLC_2, resonant tank input voltage V_{HB}, and output voltage V_o of five operating points. It can be

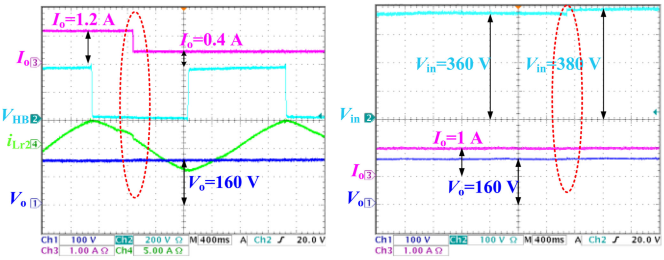

(a) (b)

Fig. 21. Dynamic response of the proposed converter at the CV charge mode. (a) When output power changes from 192 to 64 W. (b) When input voltage changes from 360 to 380 V.

seen that the diode current decreases to zero before the commutation occurs. So, the ZCS operation for both diode rectifiers of LLC_1 and LLC_2 are achieved during the whole operation range.

Based on Figs. 19 and 20, one can conclude that during the whole operation range the following statements hold.

1) LLC_1 is always operating at the series resonant frequency point. Its output voltage is almost kept constant at 95 V, and its resonant inductor current is lower than 3 A, which agrees with the theoretical analysis. As shown in Fig. 12, by selecting the magnetizing inductor $L_{m1} = 200\,\mu$H, the resonant current is below 3 A.
2) The output voltage of LLC_2 increases from 26 to 69 V during the CC charge mode to meet the voltage gain requirement.
3) The proposed converter can achieve CC charge and CV charge.
4) The ZVS operation is achieved for the whole operation range.
5) Since the switching frequency is designed below the series resonant frequency, the ZCS operation is achieved for the rectifiers during the whole operation range.

Next, the dynamic response of the proposed converter is investigated. Fig. 21 shows the dynamic response of the proposed converter for different conditions at the CV charge mode: when output power changes from 192 to 64 W; and when input voltage changes from 360 to 380 V. It can be seen that the output voltage remains constant when the output power changes, both the output voltage and output current remain constant when input voltage changes, and the proposed system provides fast dynamic response.

Similarly, Fig. 22 shows the dynamic response at the CC charge mode when output power changes and input voltage changes. It can be seen that the dynamic response of the proposed converter is good.

Fig. 23 shows the efficiency curve of the proposed converter. Since the output power level is relatively low, the efficiency is low at light load. However, for higher output power levels, the system efficiency is above 92%, and the maximum measured efficiency is around 95.5% when the output power equals 300 W. In addition, it can be seen that the efficiency of LLC_1 is about 5% higher than that of LLC_2 since LLC_1 is always operating at the series resonant frequency, which is highest efficiency operating point for *LLC* resonant converters. Its maximum efficiency is measured around 98%.

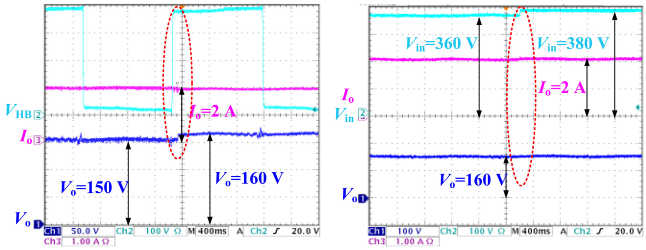

(a) (b)

Fig. 22. Dynamic response of the proposed converter at the CC charge mode. (a) When output power changes from 300 to 320 W. (b) When input voltage changes from 360 to 380 V.

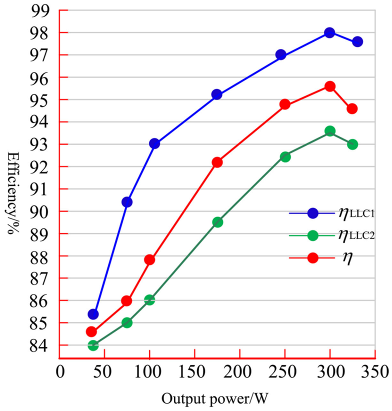

Fig. 23. Efficiency curve of the proposed converter.

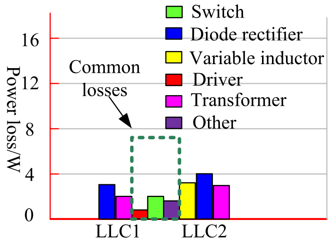

Fig. 24. Power loss analysis when $P_o = 320$ W.

Fig. 24 shows the estimated power loss analysis of the converter when $P_o = 320$ W. It can be seen that since the ZVS operation is achieved for primary switches, only the conduction losses are included; for the secondary diode rectifiers, the ZCS operation is achieved, but the conduction losses cannot be ignored due to the relatively high rms current that flows through the rectifier and the high forward voltage of the diode. In a future work, synchronous rectifier technology, low forward voltage diode, and half-bridge rectifier can be adopted to further improve the system efficiency. For the variable inductor, both the control winding loss and core loss are included.

Table IV shows the comparison results between different control strategies and topologies of an *LLC* or dual *LLC* resonant converter. Based on the comparison results, the proposed dual

TABLE IV
COMPARISON BETWEEN THE PROPOSED TOPOLOGY AND EXISTING TOPOLOGIES

Topology	Conventional LLC [8]	Modified structure [16]	Dual-bridge LLC [17]	Dual full-bridge LLC[18]	Proposed
Additional switch	0	2	2	1	0
Switching loos of additional switch	None	High	High	None	None
Number of rectifier network	1	2	1	2	2
Number of transformer	1	2	1	2	2
Number of resonant components	3	4	3	7	6
Modulation	FM	FM	PWM	FM	MC
Switching frequency	Wide range	Medium range	Fixed	Small range	Fixed
Soft switching for the primary switches	ZVS	ZVS	ZVS	ZVS	ZVS
Soft switching for the secondary rectifiers	ZCS	ZCS	ZCS	ZCS	ZCS
Control scheme	Simple	Complex	Complex	Medium	Simple

half-bridge *LLC* resonant converter with MC has the following advantages:

1) fixed switching frequency operation, which simplifies the magnetic components and driver circuits design;
2) no additional switch is required, so no extra loss is generated, and no corresponding control circuit is needed; and
3) by using two *LLC* resonant networks and the function decoupling idea, the system efficiency can be improved.

V. CONCLUSION

In this paper, a dual half-bridge *LLC* resonant converter with MC for battery charger application is proposed. The half-bridge inverter is shared between two *LLC* resonant converters, with their inputs connected in parallel, whereas their outputs are connected in series. One of the *LLC* resonant converters is designed to operate at the series resonant frequency point, where the output voltage is independent of the load. Second *LLC* resonant converter adopts MC to regulate the output of the system to provide CC charge and CV charge to the battery. In addition, the function decoupling idea is implemented to further improve the system efficiency. Since LLC_1 is operating at the best efficiency operating point, it handles most of the output power, and the main responsibility of LLC_2 is to achieve closed-loop control. By carefully designing the resonant networks, the ZVS operation for primary switches and ZCS operation for the secondary diodes can be guaranteed. Finally, a 320-W experimental prototype is built to verify the theoretical analysis. It can be seen from the experimental waveforms that the proposed converter can achieve CC charge and CV charge and the experimental results agree with the theoretical analysis. Moreover, the proposed converter has good dynamic characteristic.

The main contribution of this paper lies in the following aspects:

1) a new dual-half bridge *LLC* resonant converter for battery charger application is proposed;
2) constant output voltage and constant output current characteristics of the *LLC* resonant converter are investigated; and
3) design considerations for an *LLC* resonant converter with MC are presented.

REFERENCES

[1] M. Yilmaz and P. T. Krein, “Review of battery charger topologies, charging power levels, and infrastructure for plug-in electric and hybrid vehicles,” *IEEE Trans. Power Electron.*, vol. 28, no. 5, pp. 2151–2169, May 2013.

[2] M. Ehsani, Y. Gao, S. E. Gay, and A. Emadi, *Modern Electric Hybrid Electric and Fuel Cell Vehicles*. FL, Boca Raton, USA: CRC Press, 2005.

[3] A. Y. Saber and G. K. Venayagamoorthy, “One million plug-in electric vehicles on the road by 2015,” *Proc. IEEE Intell. Transp. Syst. Conf.*, Oct. 2009, pp. 141–147.

[4] R. Beiranvand, B. Rashidian, M. R. Zolghadri, and S. M. H. Alavi, “Using *LLC* resonant converter for designing wide-range voltage source,” *IEEE Trans. Ind. Electron.*, vol. 58, no. 5, pp. 1746–1756, May 2011.

[5] J. Deng, S. Li, C. C. Mi, and R. Ma, “Design methodology of *LLC* resonant converter for electric vehicle battery chargers,” *IEEE Trans. Veh. Technol.*, vol. 63, no. 4, pp. 1581–1592, May 2014.

[6] J. Deng, C. C. Mi, R. Ma, and S. Li, “Design of *LLC* resonant converters based on operation-mode analysis for level two PHEV battery chargers,” *IEEE/ASME Trans. Mechatronics*, vol. 20, no. 4, pp. 1595–1606, Aug. 2015.

[7] F. Musavi, M. Craciun, D. S. Gautam, and W. Eberle, “Control strategies for wide output voltage range *LLC* resonant DC–DC converters in battery chargers,” *IEEE Trans. Veh. Technol.*, vol. 63, no. 3, pp. 1117–1125, Mar. 2014.

[8] F. Musavi, M. Craciun, D. S. Gautam, W. Eberle, and W. G. Dunford, “An *LLC* resonant DC-DC converter for wide output voltage range battery charging applications,” *IEEE Trans. Power Electron.*, vol. 28, no. 12, pp. 5437–5445, Dec. 2013.

[9] G. Cao, W. Dou, K. Sun, and Y. Wang, “Design optimization of *LLC* converter for battery charger with wide output voltage range,” in *Proc. IEEE 27th Int. Symp. Ind. Electron.*, 2018, pp. 1182–1187.

[10] X. Dan Gumera, A. Caberos, and S. Huang, “Design and implementation of a high efficiency cost effective EV charger using *LLC* resonant converter,” in *Proc. Asian Conf. Energy, Power Transp. Electrific.*, 2017, pp. 1–6.

[11] Z. Fang, T. Cai, S. Duan, and C. Chen, “Optimal design methodology for resonant converter in battery charging applications based on time-weighted average efficiency,” *IEEE Trans. Power Electron.*, vol. 30, no. 10, pp. 5469–5483, Oct. 2015.

[12] Z. Li, T. Wu, G. Zhang, and R. Yang, “Hybrid modulation method combining variable frequency and double phase-shift for a 10 kW *LLC* resonant converter,” *IET Power Electron.*, vol. 11, no. 13, pp. 2161–2169, 2018.

[13] X. Yudi, M. Xingkui, Z. Zhe, and Y. Shi, “New hybrid control for wide input full-bridge *LLC* resonant DC/DC converter,” in *Proc. 3rd Int. Conf. Intell. Green Building Smart Grid*, 2018, pp. 1–4.

[14] J. H. Kim, C. E. Kim, J. K. Kim, J. B. Lee, and G. W. Moon, “Analysis on load-adaptive phase-shift control for high efficiency full-bridge resonant converter under light-load conditions,” *IEEE Trans. Power Electron.*, vol. 31, no. 7, pp. 4942–4955, Jul. 2016.

[15] B. McDonald and F. Wang, “*LLC* performance enhancements with frequency and phase shift modulation control,” *Proc. IEEE Appl. Power Electron. Conf. Expo.*, Mar. 2014, pp. 2036–2040.

[16] H. Hu, X. Fang, F. Chen, Z. J. Shen, and I. Batarseh, “A modified high-efficiency *LLC* converter with two transformers for wide input-voltage range application,” *IEEE Trans. Power Electron.*, vol. 28, no. 4, pp. 1946–1960, Apr. 2013.

[17] X. Sun, X. Li, Y. Shen, B. Wang, and X. Guo, “A dual-bridge *LLC* resonant converter with fixed-frequency PWM control for wide input applications,” *IEEE Trans. Power Electron.*, vol. 32, no. 1, pp. 69–80, Jan. 2017.

[18] H. Vu and W. Choi, “A novel dual full-bridge *LLC* resonant converter for CC and CV charges of batteries for electric vehicles,” *IEEE Trans. Ind. Electron.*, vol. 65, no. 3, pp. 2212–2225, Mar. 2018.

[19] V. S. Costa, M. S. Perdigão, A. S. Mendes, and J. M. Alonso, “Evaluation of a variable-inductor-controlled *LLC* resonant converter for battery charging applications,” in *Proc. 42nd Annu. Conf. IEEE Ind. Electron. Soc.*, 2016, pp. 5633–5638.

[20] J. M. Alonso, M. S. Perdigão, D. G. Vaquero, A. J. Calleja, and E. S. Saraiva, “Analysis, design, and experimentation on constant-frequency DC-DC resonant converters with magnetic control,” *IEEE Trans. Power Electron.*, vol. 27, no. 3, pp. 1369–1382, Mar. 2012.

[21] J. M. Alonso, G. Martínez, M. Perdigão, M. R. Cosetin, and R. N. do Prado, “A systematic approach to modeling complex magnetic devices using SPICE: Application to variable inductors,” *IEEE Trans. Power Electron.*, vol. 31, no. 11, pp. 7735–7746, May 2016.

[22] J. M. Alonso, M. S. Perdigão, G. Z. Abdelmessih, M. A. Dalla Costa, and Y. Wang, “SPICE modeling of variable inductors and its application to single inductor LED driver design,” *IEEE Trans. Ind. Electron.*, vol. 64, no. 7, pp. 5894–5903, Dec. 2016.

[23] Y. Wei, Q. Luo, S. Chen, Q. He, and L. Zhou, “A high efficiency single stage bi-directional battery charger with magnetic control,” in *Proc. IEEE Int. Power Electron. Appl. Conf. Expo.*, 2018, pp. 1–6.

[24] Y. Wei, N. Altin, Q. Luo, and A. Nasiri, “A high efficiency, decoupled on-board battery charger with magnetic control,” in *Proc. 7th Int. Conf. Renewable Energy Res. Appl.*, 2018, pp. 920–925.

[25] H. Choi, “Analysis and design of *LLC* resonant converter with integrated transformer,” in *Proc. 22nd Annu. IEEE Appl. Power Electron. Conf. Expo.*, 2007, pp. 1630–1635.

[26] M. Noah, T. Shirakawa, K. Umetani, J. Imaoka, M. Yamamoto, and E. Hiraki, “Effects of secondary leakage inductance on the LLC resonant converter—Part I: Transformer voltage gain and efficiency,” in *Proc. IEEE Appl. Power Electron. Conf. Expo.*, Anaheim, CA, USA, 2019, pp. 780–786.

[27] W. Feng and F. C. Lee, “Optimal trajectory control of *LLC* resonant converters for soft start-up,” *IEEE Trans. Power Electron.*, vol. 29, no. 3, pp. 1461–1468, Mar. 2014.

Yuqi Wei (S’18) was born in Henan, China, in 1995. He received the B.S. degree in electrical engineering from Yanshan University, Hebei, China, in 2016, the M.S. degree in electrical engineering from the University of Wisconsin-Milwaukee, Milwaukee, WI, USA, in 2018, and the second M.S. degree in electrical engineering from Chongqing University, Chongqing, China, in 2019. He is currently working toward the Ph.D. degree from the University of Arkansas, Fayetteville, AR, USA.

His current research interests include topology, modeling and control of power converters, and applications for battery charger converters.

Quanming Luo (M’14) was born in Chongqing, China, in 1976. He received the B.S., M.S., and Ph.D. degrees in electrical engineering from Chongqing University, Chongqing, China, in 1999, 2002, and 2008, respectively.

From 2002 to 2005, he was a Research and Development Engineer with Emerson Network Power Co. Ltd., Shenzhen, China. Since 2005, he has been with the College of Electrical Engineering, Chongqing University, where he is currently a Professor. He is the author or co-author of more than 40 papers in journal or conference proceedings. His current research interests include LED driving systems, communication power systems, power harmonic suppression, and power conversion systems in electrical vehicles.

Xiong Du (M’13) received the B.S., M.S., and Ph.D. degrees in electrical engineering from Chongqing University, Chongqing, China, in 2000, 2002, and 2005, respectively.

Since 2002, he has been with Chongqing University, where he is currently a Full Professor at the School of Electrical Engineering. From July 2007 to 2008, he was a Visiting Scholar with Rensselaer Polytechnic Institute, Troy, NY, USA. His research interests include power electronics system reliability and stability. He is a recipient of the National Excellent Doctoral Dissertation of P.R. China in 2008.

Necmi Altin (M’11–SM’19) received the B.Sc., M.Sc., and Ph.D. degrees from Gazi University, Ankara, Turkey, in 2000, 2003, and 2009, respectively.

He joined the Department of Electrical and Electronics Engineering, Faculty of Technology, Gazi University, as an Assistant Professor and was promoted to Associate Professor in 2014. He was a Visiting Scholar with the University of Wisconsin-Milwaukee, Milwaukee, WI, USA, between 2017 and 2019. His current research interests include power electronics, application of power electronics in renewable energy systems, high-power factor rectifiers, grid interactive inverters, and control systems.

Dr. Altin is currently an Associate Editor for the IEEE Transactions on Industry Applications for Renewable and Sustainable Energy Conversion Systems Committee.

Adel Nasiri (SM’06) was born in Sari, Iran, in 1974. He received the B.S. and M.S. degrees in electrical engineering from Sharif University of Technology, Tehran, Iran, in 1996 and 1998, respectively, and the Ph.D. degree in electrical engineering from Illinois Institute of Technology, Chicago, IL, USA, in 2004.

From 1998 to 2001, he was with Moshanir Power Engineering Company. From 2004 to 2005, he was with ForHealth Technologies, Inc., Daytona Beach, FL, USA. He is currently a Professor and the Director with the Center for Sustainable Electrical Energy Systems, College of Engineering and Applied Sciences, University of Wisconsin–Milwaukee, Milwaukee, WI, USA. His research interests include renewable energy interface, energy storage, and microgrids. He authored or coauthored numerous technical journal and conference papers on related topics. He also has seven patent disclosures. He is a co-author of the book *Uninterruptible Power Supplies and Active Filters* (CRC Press, 2017).

Dr. Nasiri is currently the Paper Review Chair for the IEEE TRANSACTIONS ON INDUSTRY APPLICATIONS, an Editor for Power Components and Systems, and an Associate Editor of the *International Journal of Power Electronics*. He was an Editor for the IEEE TRANSACTIONS ON SMART GRID (2013–2019). He was the General Chair for 2012 IEEE Symposium on Sensorless Electric Drives, 2014 International Conference on Renewable Energy Research and Applications, and 2014 IEEE Power Electronics and Machines for Wind and Water Applications.

J. Marcos Alonso (S’94–M’98–SM’03) received the M.Sc. and Ph.D. degrees in electrical engineering from the University of Oviedo, Oviedo, Spain, in 1990 and 1994, respectively.

Since 2007, he has been a Full Professor with the Electrical Engineering Department, University of Oviedo. He is a co-author of more than 400 journal and conference publications, including around 100 publications in highly referenced journals. His research interests include lighting applications, dc–dc converters, power factor correction, resonant inverters, and power electronics in general. He is the holder of seven Spanish patents.

Prof. Alonso is currently an Associate Editor for the IEEE TRANSACTIONS ON POWER ELECTRONICS and IEEE JOURNAL ON EMERGING AND SELECTED TOPICS ON POWER ELECTRONICS. He was the Chair for the IAS Industrial Lighting and Displays Committee for the term 2017–2018. He is currently the Chair for the IAS Awards Department. He was the recipient of nine IEEE Awards.